Numerical study of the polarization proprieties
in a ring cavity with total polarization control

L. A. Rodríguez-Morales[a,*], I. Armas-Rivera[a], M. Durán-Sánchez[a,b], and B. Ibarra-Escamilla[a]

[a]*Instituto Nacional de Astrofísica, Óptica y Electrónica,*
L. E. Erro 1, Sta. Ma. Tonantzintla, Pue. 72824, México.
[b]*CONACYT-Instituto Nacional de Astrofísica, Óptica y Electrónica,*
Apartado Postal 51 y 216, 72000, Puebla, Pue., México.
beto7500@hotmail.com

We report the numerical study of the polarization properties of a net anomalous dispersion ring cavity with total polarization control. As a mode locker, we use the nonlinear polarization rotation (NPR) method. The initial ellipticity and azimuth were fixed to 0.23 rad and 0 rad, respectively. The simulations, made by the split-step Fourier method, show changes in polarization with respect to initial conditions after the mode-lock process, such as previously reported in the literature. It was found that polarization changes are caused by non-linear birefringence. The pulsed laser produces solitonic pulses with 0.4 ps FWHM and 240 W peak power.

Keywords: Mode-lock; solitons; fiber laser; NPR; polarization.

PACS: 42.60.Fc; 42.81.Dp; 42.65.Re; 05.45.Yv; 42.65.Wd

1. Introduction

Passively mode-locked fiber lasers have attracted much attention since it can operate in a wide variety of regimes [1-10], including the generation of a single soliton in the cavity [3-5]. The regime of generation depends on many factors, such as dispersion, amplification, attenuation, and nonlinearities. Many efforts have been done in the laser numerical modeling to find the dependence of generation regimes on laser parameters [11]. Some regimes such as the dissipative soliton resonance (DSR) [12] and spiny solitons [13] were predicted first by modeling. These numerical simulations have shown that many regimes can be generated in a single cavity.

The dependence experimental study of the regimes on the laser parameters is usually complicated since some laser parameters are uncertain and others, as birefringence, are difficult to eliminate or to control. One of the most important aspects is the polarization dynamics of the pulses and the birefringence of the elements included in the cavity. It has been proved that it is possible to switch between regimes through polarization controllers (PC) adjustments [14-16]; however, in most published papers, the appropriate position of the PC was found randomly.

In recent years, Kuzin *et al.* [17-18] have been dedicated to performing the experimental investigation of passive mode-lock nonlinear polarization rotation (NPR) fiber lasers with strict polarization control. In these investigations, it was possible to show the initial conditions required to generate different types of pulses in a controlled and reproducible manner. In [17], it was shown that a change in polarization after the mode-locking process occurs. It was mentioned that this behavior was due to the existence of some degree of linear birefringence still present in the cavity.

In order to fulfill these polarization investigations, we perform the numerical investigation of a passively the mode-locked fiber laser to demonstrate the origin of the polarization changes after mode-locking process caused by non-linear birefringence. The obtained results show promising advances in the investigations in the full understanding, development, and generation of different types of pulses in passively mode-locked fiber lasers.

2. Theoretical model

The proposed laser cavity under study is shown in Fig. 1. The cavity model consists of a free birefringence mode-locked ring cavity fiber laser by the NPR-technique [17-18].

To have total polarization control in the cavity, it is important to mitigate the linear birefringence in the Erbium-doped fiber amplifier (EDFA) to preserve the polarization state of the light. The model includes a double-pass EDFA as presented in [17-18]. The simulated gain was Erbium-doped fiber with a central peak centered at 1550 nm. An optical isolator is commonly used to ensure the unidirectionality of the cavity. A polarization controller (PC) is usually inserted in the cavity to change the polarization state of the light before propagation through the non-linear element. A delay line is used as a non-linear and dispersive media where the non-linear and dispersive effects interact to generate different types of dynamics in the function of different parameters as the nonlinearity, dispersion, length, pump power, and polarization of the light [17]. To ensure the total polarization control in the cavity, and therefore the NPR effect, the delay line is commonly a twist conventional SMF fiber [19]. The twisted fiber in the cavity is used to maintain constant ellipticity during propagation. Recently, some investigations have
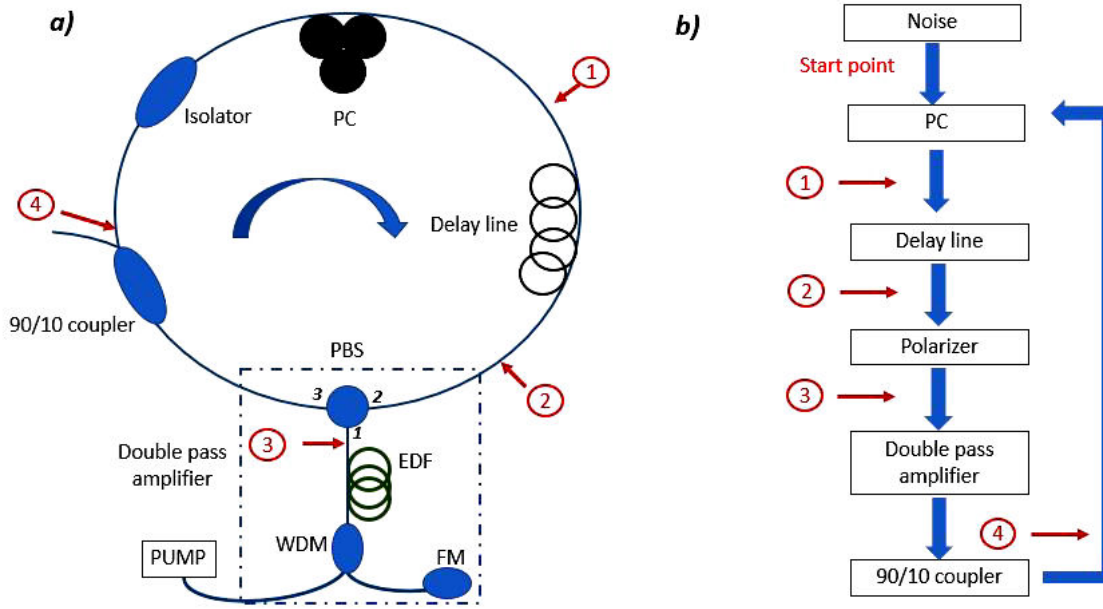
FIGURE 1. Laser cavity, a) conceptual cavity, b) effectively cavity.

shown that it is possible to mitigate the linear birefringence and even the circular birefringence produced by the twist of the fiber allowing the total control of the light polarization no matter the environmental conditions [20]. Finally, a polarization beam splitter (PBS) is used as a polarizer. The PB'S use necessary to build the double-pass amplifier detailed in [18]; the PBS contains three ports. When light enters through port 1, the beam is divided into two orthogonal linear polarization components that travel to ports 2 and 3, respectively. On the other hand, when incident light with any state of polarization enters through port 2, only one linear component passes through the PBS to port 1, working as a polarizer. This component travels through the EDF, changing its polarization due to the fiber birefringence; then the light is reflected in a Faraday Mirror (FM). The reflected light has a polarization orthogonal to that of the incident light. The light then travels back through the birefringent fiber and returns to port 1 of the PBS with a linear polarization orthogonal to that of the incident light so that it transfers to port 3 of the PBS. The light after the port 3 of the PBS had been amplified, a coupler, 90/10 in our case, is used as the cavity exit.

To start the simulation, we begin with the place marked as a start point in Fig. 1b). The initial signal is a noise signal, created by a photon in every frequential point of the computational window, and the numerical model is solved by a split-step Fourier method. We took step sized small enough to be sure that the parts of the solution with sharply growing amplitudes are finely discretized along both z and t axes; more precisely, we use 212 mesh points in the transverse direction to sample the t-interval up to [- 150, 150], that is sufficiently large to have practically zero values of the evolve function at its edges. The first step in the cavity effectively is a PC; the mathematical expression used to transform every polarization

state described by a Jones vector in circular basis,

$$\mathbf{E}_{in} = \left[\begin{array}{c} A_+ \\ A_- \end{array} \right],$$

to a polarization state with ellipticity e and azimuth ϕ, is given by:

$$E_{pc} = \sqrt{P_T} \left[\begin{array}{c} \sqrt{P_T} \exp(i\phi) \\ \sqrt{P_T} \exp(-i\phi) \end{array} \right] \tag{1}$$

where $P_T = \sqrt{|A_+|^2 + |A_-|^2}$ and

$$P_r = \frac{(1+e)^2}{2(1+e^2)}, \quad P_l = 1 - P_r. \tag{2}$$

The delay line of length Z was modeled by the coupled nonlinear Schödinger equations in circular basis given by:

$$\frac{\partial A_+}{\partial z} + \beta_1 \frac{\partial A_+}{\partial t} + \frac{i\beta_2}{2} \frac{\partial^2 A_+}{\partial t^2} + \frac{\alpha}{2} A_+$$
$$= \frac{i\Delta\beta}{2} A_- + \frac{2i\gamma}{3}(|A_+|^2 + 2|A_-|^2)A_+, \tag{3}$$

$$\frac{\partial A_-}{\partial z} + \beta_1 \frac{\partial A_-}{\partial t} + \frac{i\beta_2}{2} \frac{\partial^2 A_-}{\partial t^2} + \frac{\alpha}{2} A_-$$
$$= \frac{i\Delta\beta}{2} A_+ + \frac{2i\gamma}{3}(|A_-|^2 + 2|A_+|^2)A_-. \tag{4}$$

β_1, β_2 are the first and second-order dispersion coefficients, $\Delta\beta$ is the linear birefringence, α is a linear loss and γ is the nonlinear coefficient in both Eqs. (3) and (4), the linear and circular birefringence effects are misprized because of the fiber is considered a bi-twist fiber [20]. The value of the coefficients used for the delay line is shown in Table I.

TABLE I. Delay line parameters.

Coefficients	Values
β_1	1×10^{-9} ps/ km
β_2	-20 ps^2/ km
α	0
γ	1.5 1/W * km
$\Delta\beta$	0
Z	50 m

The double-pass amplifier is model as a gain, which depends on frequency ω, and considering the gain saturation effect:

$$g = \frac{g_0}{1 + \dfrac{E_{\text{pulse}}}{E_{\text{sat}}}} \quad (5)$$

3. Simulation results and analysis

To start the simulation, we fixed some crucial initial parameters as all-polarization control cavities that the authors mentioned in [17], the pump power, the ellipticity, and the azimuth of the polarization ellipse. For specific parameters shown in Table II, we find solitonic pulses, the normalized spectrum, and the temporal profile are shown in Fig. 2.

Figure 2 a) present the normalized spectrum in point marked as number 4 in Fig. 1, before the output coupler. The spectrum is centered at 1550 nm and has a full width at half-

TABLE II. Initial cavity parameters.

ellipticity (e)	13°~0.23 rad
Azimuth (ϕ)	0 rad
g_0	40 m^{-1}
E_{sat}	0.03 J
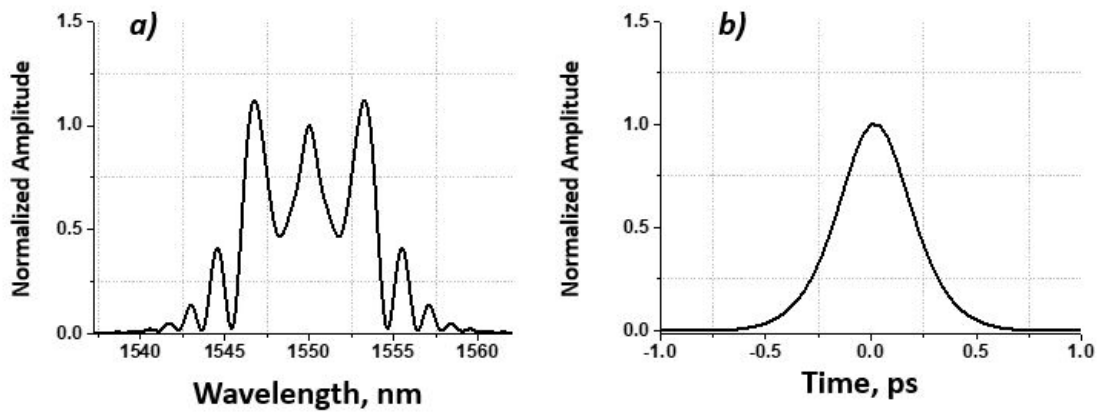
2.JPG

FIGURE 2. a) Spectral profile and b) temporal profile.
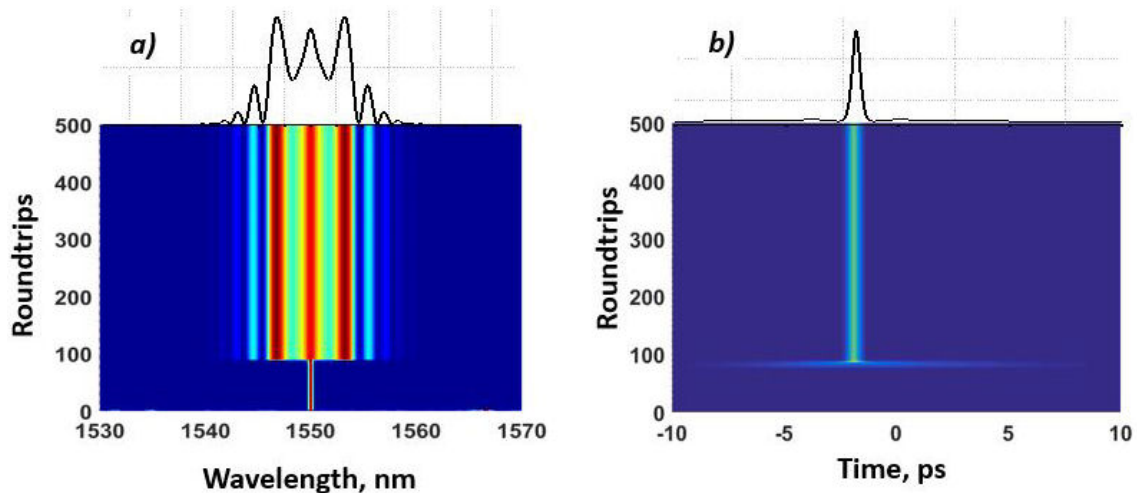
FIGURE 3. 500 Roundtrips evolution, a) spectrum, b) time trace.
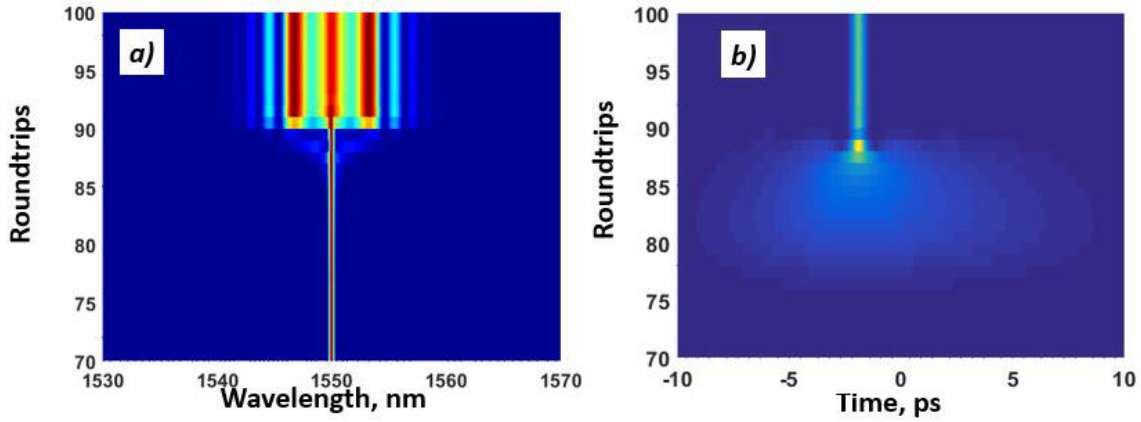
FIGURE 4. Mode-locked convergence, a) spectral behavior, b) time behavior.
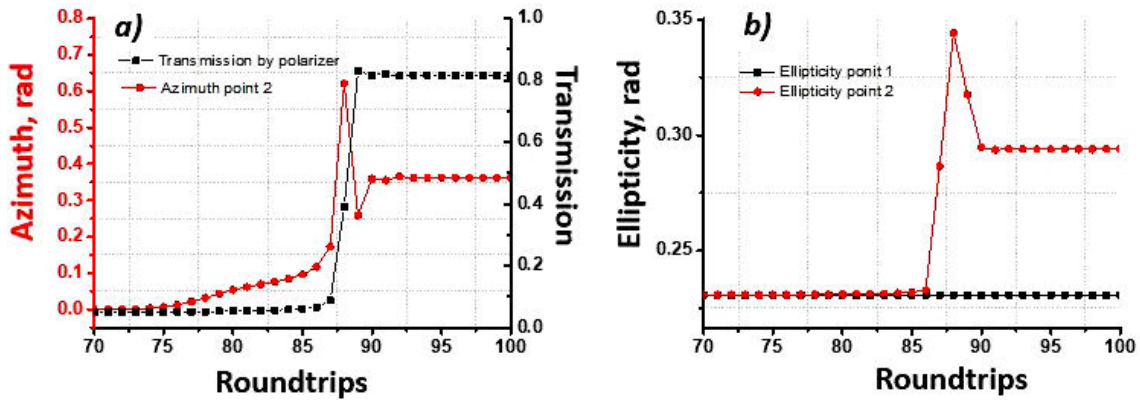
FIGURE 5. a) Azimuth changes because of NPR (red dots), transmission through the polarizer (black squares), b) ellipticity, initial at point 1 (red dots), final at point 2 (black squares).

maximum (FWHM) of 2.95 nm. It has a typical shape for soliton mode-locking with symmetrical Kelly's sidebands. The amplitude of Kelly's sidebands could vary, changing dissipative terms and the spectral filtering [20,21]. The temporal profile is shown in Fig. 2 b), the FWHM is around 0.40 ps.

In order to show the evolution and the stabilization of the laser, a 500 roundtrips analysis is presented in Fig. 3.

Figure 3 shows the formation and evolution of a mode-locked pulse, a soliton from a noise signal. In simulations, a noise wave is assumed as an initial value. We can have a formed soliton after several round-trips. Figure 3 a) shows the spectral behavior within the first 500 roundtrips, some roundtrips after starting the laser operation, the noise signal converges to a narrow signal in the frequency domain, before the mode-locked occurs. Once the pulsed behavior has begun, the signal is broadened, less than ten roundtrips are necessary to adopt the final spectral shape, after 100 turns the signal is stable. On the other hand, Fig. 3b) shows the soliton trajectory in a round-trip. The energy is distributed throughout the time window, becoming narrower roundtrip by roundtrip until it converges to a temporal FWHM less than 1 ps after 100 roundtrips. The pulse presents the same time width roundtrip by roundtrip, a stable pulsed signal.

In order to see in detail when the mode-locked process

occurs, a close-up from the 70 to 100 roundtrip is presented in Fig. 4. We can observe in Fig. 4 a) that after the 85th roundtrip, the spectral peak power begins to collapse in a broader spectrum, while in Fig. 4 b) the opposite happens, the temporal energy is distributed in a width temporal area, abruptly the temporal trace begins to narrow until it collapses into a pulse of 0.4 ps FWHM with constant amplitude after the 90th roundtrip.

Three points of interest were fixed, red numbers in Fig. 1 reveal the points, number 1 indicates the point after PC, this point is crucial to know the state of polarization before the propagation, the circle labeled with number 2 indicates some light properties after propagation, we are interested in the polarization state, this will give us a clue of the non-linear birefringence induced by the delay line; finally, point 3 is destined to study the transmission through the polarizer, so we can be able to know how the saturable absorber works. The polarization properties were calculated by the stokes parameters in circular basis.

$$S_0 = |a_+|^2 + |A_-|^2, \quad S_1 = -\frac{2Re(A_+^* A_-)}{S_0}$$

$$S_2 = \frac{|a_+|^2 - |A_-|^2}{S_0}, \quad S_3 = \frac{2Im(A_+^* A_-)}{S_0}. \quad (6)$$
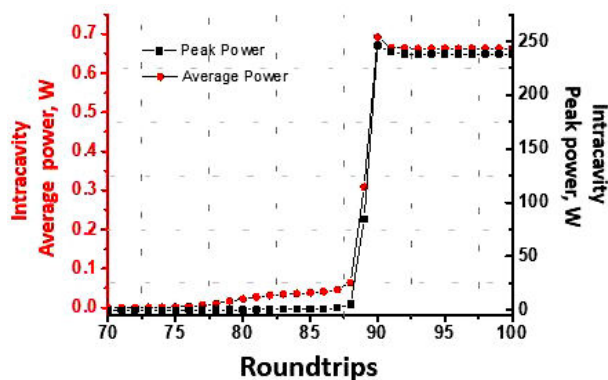
FIGURE 6. Intracavity power, average (red dots), peak (black squares).

Figure 5a) shows the azimuth in point 2, red dots, because of the NPR effect, the polarization ellipse rotates, the NPR rotation is proportional to the peak power, ellipticity, and the fiber length. The 75th roundtrip is a crucial lap for mode-locking, the polarization ellipse begins to rotate starting this lap, the saturable absorber has begun to discriminate the low power components, turn by turn the pulse power increases, as a consequence the azimuth rotates linearly until lap 87, after this point the saturable absorber makes a radical power discrimination, sharp jump around 0.61 rad rotation is present, subsequently the gains and non-linear losses are immobilized in the next 5 laps, once the 95th laps are achieved, the laser has finished discriminating low powers, reaching the stabilization. The azimuth changes impact the transmission through the polarizer, Fig. 5 a), black squares, although the transmission slope is less than the azimuth slope, the threshold for the abrupt change is lap 87. The transmission through the polarizer gives us an idea about the pulse energy, this specific case with the initial conditions of the light beam at point 1, pumping and polarization, the maximum reached transmission is close to 80%, this percentage can be altered by changing these initial conditions generating different types of pulses as shown in [17].

An important result is shown in Fig. 5b): in cavities with total polarization control it was supposed the ellipticity before and after the mode-locking does not change although experimental results report this change, the authors mention the ellipticity changes before and after mode-lock are generated by residual linear birefringence in the fibers used, in our model the linear birefringence has been eliminated, however, it was found that the ellipticity changes from 0.23 rad to 0.29 rad after mode-lock due to non-linear birefringence, in Fig. 5b) the starting ellipticity is different to the ellipticity after the propagation once the mode-lock process is started, as a result of this ellipticity change, the NPR effect would have to be affected roundtrip by roundtrip during the mode-lock process, affecting previously assumed behavior, opening a gap in the study of polarization in the mode-lock cavities with total polarization control. The ellipticity and azimuth have a repercussion in the formed pulse power. Figure 6 shows the intracavity average and peak power in the mode-lock process; the data for Fig. 6 is taken in point 4 in Fig. 1.

The average power change before mode-lock has a slope slightly greater than the peak power slope can be explained with the temporal pulse behavior showed in Fig. 4 b), and the temporal width is greater than the change in amplitudes. Again, it is shown that this type of cavities can form stable power pulses as shown in Fig. 6 after the 95th roundtrip.

4. Conclusion

We have numerically studied an NPR ring mode-locked cavity with total polarization control. Under fixed initial polarization conditions, we were able to find a solitonic pulse. The polarization of the pulse was studied before and after the mode-lock process, by the roundtrip method into the ring. We found that the azimuth jumps from 0 rad to 0.36 rad and the ellipticity from 0.23 rad to 0.29 rad. Numerically, we found similar results to the one reported in [17]. In contrast to the assumptions by the mentioned authors, it has been found that changes in polarization after mode-lock are not caused by imperfections in the experimental setup, they are caused by nonlinear birefringence.

1. P. Grelu and N. Akhmediev, Dissipative solitons for mode-locked lasers, *Nat. Photonics* **6** (2012) 84. https://doi.org/10.1038/nphoton.2011.345

2. F. Sanchez *et al*., Manipulating dissipative soliton ensembles in passively mode-locked fiber lasers, *Opt. Fiber Technol.* **20** (2014) 562. https://doi.org/10.1016/j.yofte.2014.06.009

3. I. N. Duling, All-fiber ring soliton laser mode locked with a nonlinear mirror, *Opt. Lett.* **16** (1991) 539. https://doi.org/10.1364/OL.16.000539

4. F. Krausz, T. Brabec, and C. Spielmann, Self-starting passive mode locking, *Opt. Lett.* **16** (1991) 235. https://doi.org/10.1364/OL.16.000235

5. V. J. Matsas, D. J. Richardson, T. P. Newson, and D. N. Payne, Characterization of a self-starting, passively mode-locked fiber ring laser that exploits nonlinear polarization evolution, *Opt. Lett.* **18** (1993) 358. https://doi.org/10.1364/OL.18.000358

6. D. Y. Tang, L. M. Zhao, B. Zhao, and A. Q. Liu, Mechanism of multisoliton formation and soliton energy quantization in passively mode-locked fiber lasers, *Phys. Rev. A* **72** (2005) 043816. https://doi.org/10.1103/PhysRevA.72.043816

7. Ph. Grelu and J. M. Soto-Crespo, Multisoliton states and pulse fragmentation in a passively mode-locked fibre laser, *J. Opt. B Quantum Semiclassical Opt.* **6** (2004) S271. `https://doi.org/10.1088/1464-4266/6/5/015`

8. D. Y. Tang, W. S. Man, H. Y. Tam, and P. D. Drummond, Observation of bound states of solitons in a passively mode-locked fiber laser, *Phys. Rev. A* **64** (2001) 033814.

9. P. Grelu, F. Belhache, F. Gutty, and J.-M. Soto-Crespo, Phase-locked soliton pairs in a stretched-pulse fiber laser, *Opt. Lett.* **27** (2002) 966. `https://doi.org/10.1364/OL.27.000966`

10. P. Grelu, F. Belhache, F. Gutty, and J. M. Soto-Crespo, Relative phase locking of pulses in a passively modelocked fiber laser, *J. Opt. Soc. Am. B* **20** (2003) 863. `https://doi.org/10.1364/JOSAB.20.000863`

11. Y. Kwon, L. A. Vazquez-Zuniga, S. Lee, H. Kim, and Y. Jeong, Numerical study on multi-pulse dynamics and shot-to-shot coherence property in quasi-mode-locked regimes of a highly-pumped anomalous dispersion fiber ring cavity, *Opt. Express* **25** (2017) 4456. `https://doi.org/10.1364/OE.25.004456`

12. N. Akhmediev, J. M. Soto-Crespo, and Ph. Grelu, Roadmap to ultra-short record high-energy pulses out of laser oscillators, *Phys. Lett. A* **372** (2008), 3124. `https://doi.org/10.1016/j.physleta.2008.01.027`

13. W. Chang, J. M. Soto-Crespo, P. Vouzas, and N. Akhmediev, Spiny solitons and noise-like pulses, *J. Opt. Soc. Am. B* **32** (2015) 1377. `https://doi.org/10.1364/JOSAB.32.001377`

14. X. Zou, J. Qiu, X. Wang, Z. Ye, J. Shi, and J. Wu, Versatile mode-locked fiber laser with switchable operation states of bound solitons, *Appl. Opt.* **55** (2016) 4323. `https://doi.org/10.1364/AO.55.004323`

15. M. Han, S. Zhang, X. Li, H. Zhang, H. Yang, and T. Yuan, Polarization dynamic patterns of vector solitons in a graphene mode-locked fiber laser, *Opt. Express* **23** (2015) 2424.

16. V. Tsatourian *et al.*, Polarisation Dynamics of Vector Soliton Molecules in Mode Locked Fibre Laser, *Sci. Rep.* **3** (2013) 3154. `https://doi.org/10.1038/srep03154`

17. H. Santiago-Hernández *et al.*, Initial conditions for dissipative solitons in a strict polarization-controlled passively mode-locked Er-Fiber laser, *Opt. Express* **25** (2017) 25036. `https://doi.org/10.1364/OE.25.025036`

18. L. A. Rodriguez-Morales *et al.*, *Dual-wavelength quasi-mode-locked regimes of an Er-doped fiber ring laser OSA Continuum* **1** (2018) 416. `https://doi.org/10.1364/OSAC.1.000416`

19. Almanee M, Haus JW, Armas-Rivera I, Beltrán-Pérez G, Ibarra-Escamilla B, Duran-Sanchez M, Álvarez-Tamayo R. I., Kuzin EA, Bracamontes-Rodríguez YE, Pottiez O. Polarization evolution of vector wave amplitudes in twisted fibers pumped by single and paired pulses. *Opt Lett.* **41** (2016) 4927. `https://doi.org/10.1364/OL.41.004927`

20. L. A. Rodríguez-Morales *et al.*, Experimental investigation of polarization imbalanced nonlinear loop mirror with double-sense twisted fiber as a filter to clean up solitons, *J. Opt.* **20** (2018) 015502. `https://doi.org/10.1088/2040-8986/aa9af8`

21. J. P. Gordon, Dispersive perturbations of solitons of the nonlinear SchrÃ¶dinger equation. *Journal of the Optical Society of America B*, **9** (1992) 91. `https://doi.org/10.1364/JOSAB.9.000091`

22. I. Armas-Rivera *et al.*, Wide wavelength-tunable passive mode-locked Erbium-doped fiber laser with a SESAM, *Optics & Laser Technology*, **134** (2021) 106593. `https://doi.org/10.1016/j.optlastec.2020.106593`